J. Am. Ceram. Soc., 93 [12] 3997–4000 (2010)
DOI: 10.1111/j.1551-2916.2010.04193.x

journal

Novel Synthesis of Hierarchical Tungsten Carbide Micro-/Nanocrystals from a Single-Source Precursor

Deliang Chen,[†,‡,§] Hejing Wen,[‡] Haitao Zhai,[‡] Hailong Wang,[‡] Xinjian Li,[§] Rui Zhang,[‡,¶] Jing Sun,[‖] and Lian Gao[‖]

[‡]School of Materials Science and Engineering, Zhengzhou University, Zhengzhou 450001, China

[§]School of Physics and Engineering, Zhengzhou University, Zhengzhou 450001, China

[¶]Laboratory of Aeronautical Composites, Zhengzhou Institute of Aeronautical Industry Management, Zhengzhou 450046, China

[‖]The State Key Laboratory of High Performance Ceramics and Superfine Microstructure, Shanghai Institute of Ceramics, Chinese Academy of Sciences, Shanghai 200050, China

Hierarchical tungsten carbide (WC) micro-/nanocrystals were synthesized by thermal treating a single-source precursor of the tungstate-based inorganic–organic hybrid compound in a sealed quartz tube at 1000°–1050°C. The hybrid precursor was synthesized by an acid–base reaction of H_2O-moistened H_2WO_4 and *n*-octylamine in a nonpolar solvent. The X-ray diffraction results indicated that the product obtained at 1050°C for 2 h consisted of a hexagonal WC phase, and the products obtained at temperatures lower than 1000°C had other phases (e.g., α-W_2C, W or β-$W_{40.9}N_{9.1}$) besides the major phase of hexagonal WC. The scanning electron microscopy observations indicated that the hexagonal WC obtained at 1050°C consisted of hierarchical microparticles with a size range of 4–18 μm, and the above microparticles were porous aggregates of WC nanoparticles with crystal sizes of 100–250 nm. The newly developed process could achieve pure WC materials at relative low temperatures using a single-source precursor, and the porous and hierarchical WC micro-/nanoparticles would have potential applications in catalysis and superhard composites.

I. Introduction

Tungsten carbide (WC) has attracted considerable interest because of its high hardness, high chemical stability, and good wear/erosion resistance.[1] WC has been extensively applied in cutting and drilling tools, wear-resistant parts of machines, and hard alloy coatings.[2] WC nanocrystals are also widely used as catalysts or catalyst supports, because of their platinum-like behavior in surface catalysis.[3,4]

WC powders are usually prepared by the reaction of elemental W and C at a high temperature for a long reaction time, or by a two-step process wherein tungsten oxide is first reduced to tungsten in a hydrogen atmosphere followed by the reaction with carbon.[5] Recently, several new methods, including combustion synthesis,[6] plasma-assisted process,[7] sonochemical method,[8] microwave carburization,[9] and solid-state synthesis[10] have been developed to synthesize WC micro-/nanocrystals.[11] WC crystals with specific shapes, such as hollow microspheres,[12] porous structures,[3,4] nanotubes,[13] and inverse opal structures[14] have also been synthesized using various methods. However, these developed methods usually need multiple precursors, multiple steps, and high treating temperatures, and the synthetic processes are complex.

We herein introduce a simple and efficient process for the synthesis of hierarchical WC micro-/nanocrystals using a single-source precursor at a relatively low temperature. The single-source precursor is a tungstate-based inorganic–organic hybrid derived from a reaction of tungstite and organic amines. The phase compositions, morphologies, and microstructures of the precursors and the final products are characterized using the techniques of XRD, SEM, TG-DSC, and FT-IR. The possible formation process for WC crystals is also discussed.

II. Experimental Procedure

H_2WO_4 powders (Sinopharm Chemical Reagent Beijing Co. Ltd, AR, Beijing, China), *n*-octylamine (Sinopharm Chemical Reagent Beijing Co. Ltd, CP), heptane (Tianjin Huadong Reagent Factory, AR, Tianjin, China), and ethanol (Yantai Shuangshuang Chemical Reagent Co. Ltd., AR, Yantai, China) were used as received.

The tungstate-based inorganic–organic hybrids were synthesized by a reaction between H_2WO_4 and *n*-octylamine in heptane. Typically, 10 g of H_2WO_4 powders was moistened by 5 mL of distilled water, and the H_2O-moistened H_2WO_4 was then dispersed in a mixture of 0.4 mol of *n*-octylamine, and 530 mL of heptane under a constant magnetic stirring at room temperature. The molar ratio of H_2WO_4 to *n*-octylamine was about 1:10 and the volume ratio of *n*-octylamine to heptane was 1:8. After a reaction time of more than 48 h, the resulting white solid was collected by centrifugation, washed with ethanol, and then dried under a reduced pressure at room temperature for 30 h. The dried product, a tungstate-based inorganic–organic hybrid compound, was used as the precursor for synthesis of WC micro-/nanocrystals.

The synthesis of WC particles using the tungstate-based inorganic–organic hybrid compound as the precursor was conducted in a sealed quartz tube with a diameter of 10 mm. Typically, 0.3 g of the hybrid precursor was placed in the bottom of the quartz tube. The quartz tube was then vacuumized to 2×10^{-3} Pa and sealed. The sealed quartz tube with a length of 25 cm was placed in an electrical resistance furnace, and

H.-E. Kim—contributing editor

Manuscript No. 28342. Received July 16, 2010; approved September 13, 2010.
This work was financially supported by the National Nature Science Foundation of China, (Grant No. 50802090), the China Postdoctoral Science Foundation (Grant No. 20090450094), the Opening Project of State Key Laboratory of High Performance Ceramics and Superfine Microstructure (Grant No. SKL200905SIC), and the Introduced Talent Project of Zhengzhou University.
[†]Author to whom correspondence should be addressed. e-mail: dlchen@zzu.edu.cn

thermally treated at 750°–1050°C with a heating rate of 5°C/min for 2–10 h. After a given reaction time, the sealed tube was cooled naturally to room temperature. The black powders at the bottom of the quartz tube were carefully collected.

The phase compositions were identified by an X-ray diffraction (XRD) equipment (XD-3, Beijing Purkinje General Instrument Co. Ltd., Beijing, China). The morphologies were observed using a scanning electron microscope (SEM, JEOM-6700F, JEOL Co. Ltd., Tokyo, Japan). The specific surface areas of the products were measured using the BET method (F-Sorb 3400, Beijing Jinaipu Science and Technique Co. Ltd., Beijing, China). TG-DTA curves were recorded on a thermal analysis system (NETZSCH STA409PC, NETZSCH Instruments Co. Ltd., Leuna, Germany) with a heating rate of 5°C/min in an air flow. Fourier-transform infrared spectra (FT-IR, Nicolet 460, Thermo Nicolet Instrument Corp., WI) were applied to characterize the hybrid precursors using the KBr disk technique. The particle size distribution of the WC particles obtained was examined using a laser particle size analyzer (Microtrac-X100, Microtrac Inc., NY).

III. Results and Discussion

Figure 1 shows the XRD patterns of the commercial H_2WO_4 powders and the as-obtained tungstate-based inorganic–organic hybrid compound. As Figure 1(b) shows, the commercial H_2WO_4 powders can be attributed to an orthorhombic phase according to JCPDS No. 43-0679. As shown in Fig. 1(a), a completely new compound is obtained after the reaction of H_2WO_4 with *n*-octylamine, because a series of new reflections below 20° in 2θ occur, and no identifiable reflections in the high 2θ range are observed, which is completely different from the reflections from H_2WO_4. The reflections in the low 2θ range are characteristic of a highly ordered lamellar structure, and can be indexed to the reflections from (00*l*) diffraction planes. The XRD result therefore indicates that the as-obtained hybrid precursor is of an ordered lamellar structure. The interlayer distance can be calculated to be 2.568(5) nm according to its (00*l*) reflections by minimizing the sum of squares of the residuals in 2θ.

Figure 2 shows a typical SEM image of the tungstate-based inorganic–organic hybrid compound, obtained by a reaction of H_2O-moistened H_2WO_4 with *n*-octylamine. As shown in Fig. 2, the hybrid compound takes on a plake-like morphology, with side sizes of about 1 μm. The above plake-like morphology is very different from the belt-like morphology of the products derived from the reaction of $H_2W_2O_7 \cdot xH_2O$ with *n*-octylamine

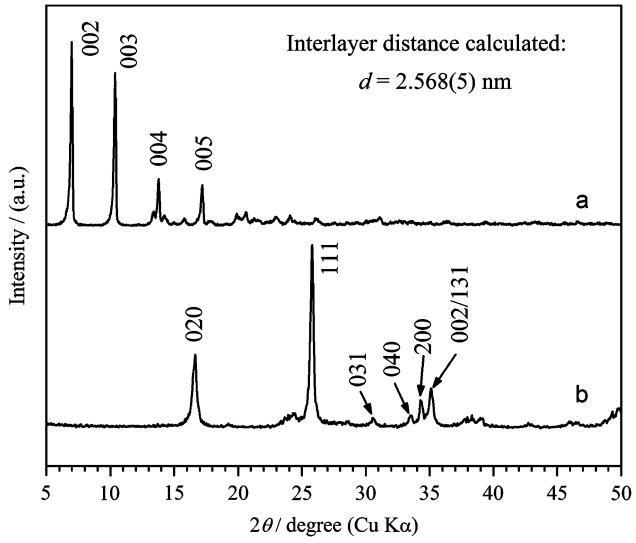

Fig. 1. The X-ray diffraction patterns of (a) the as-obtained tungstate-based inorganic–organic hybrid compound, and (b) its starting material of H_2WO_4 powders.

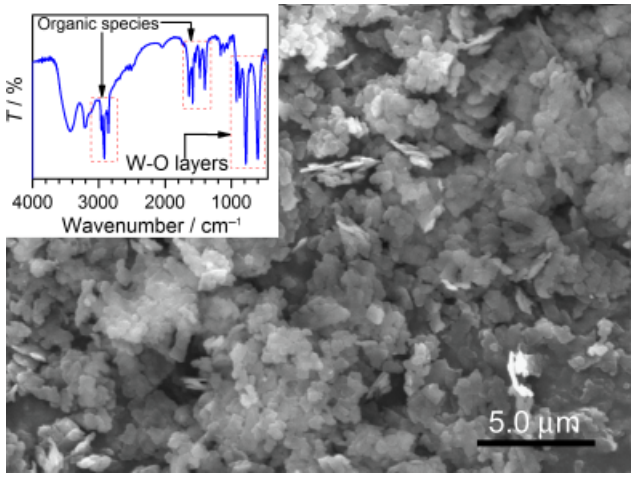

Fig. 2. A typical scanning electron microscopy image of the tungstate-based inorganic–organic hybrid compound derived from a reaction between H_2O-moistened H_2WO_4 powders and *n*-octylamine (the inset is its FT-IR spectrum).

in heptane.[15] According to the FT-IR spectrum (the inset of Fig. 2), the tungstate-based inorganic–organic hybrid compound consists of inorganic W–O layers and organic ammonium ions, indicating that it is a tungstate-based inorganic–organic layered hybrid, similar to the previously report results.[15] The

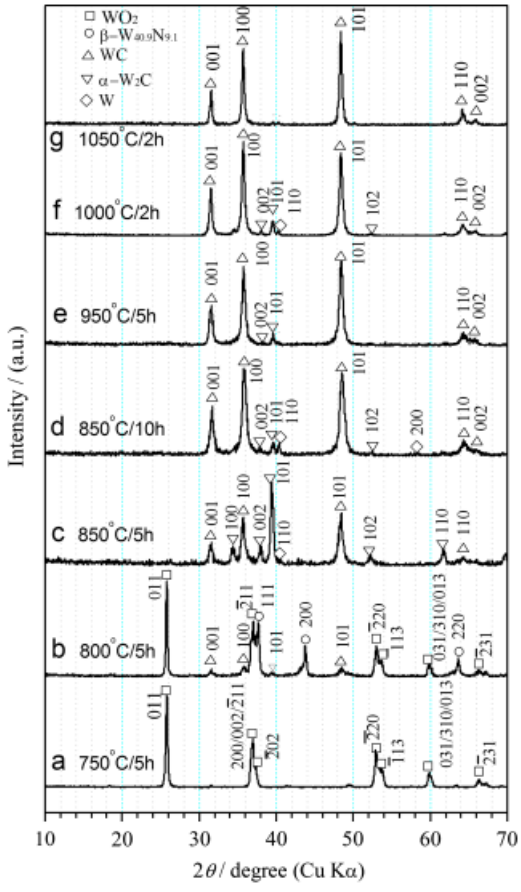

Fig. 3. The X-ray diffraction patterns of the products obtained by thermally treating the tungstate-based inorganic–organic hybrid compound in a sealed quartz tube under various conditions: (a) 750°C for 5 h, (b) 800°C for 5 h, (c) 850°C for 5 h, (d) 850°C for 10 h, (e) 950°C for 5 h, (f) 1000°C for 2 h, and (g) 1050°C for 2 h. (Δ) WC (JCPDS No. 25-1047), (∇) α-W_2C (JCPDS No. 35-0776), (◇) W (JCPDS No. 04-0806), (○) β-$W_{40.9}N_{9.1}$ (JCPDS No. 03-1031), and (□) WO_2 (JCPDS No. 32-1393).

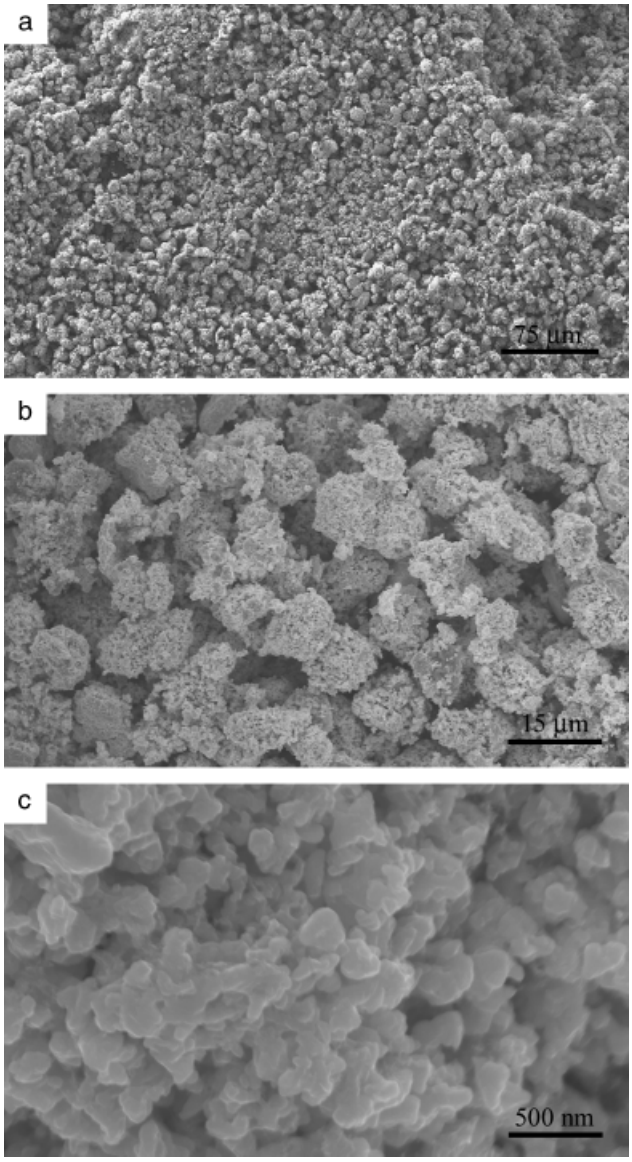

Fig. 4. Scanning electron microscopy images (a–c) with various magnifications of the WC powders obtained by treating the tungstate-based inorganic–organic hybrid compound at 1050°C for 2 h.

TG-DTA curves suggested the mass remaining is 65% after thermal treating at 600°C in an air flow.

Figure 3 shows the XRD patterns of the products obtained by thermally treating the tungstate-based inorganic–organic hybrid compound at 750°–1050°C for 2–10 h in a sealed quartz tube. As Fig. 3(a) shows, the product obtained at 750°C for 5 h can be readily indexed to monoclinic WO_2 (JCPDS No. 32-1393), and no other phases are observed. For the product obtained at 800°C for 5 h, as shown in Fig. 3(b), the phase of monoclinic WO_2 is still the main composition, but an amount of cubic β-$W_{40.9}N_{9.1}$ (JCPDS No. 03-1031) and a small amount of hexagonal WC (JCPDS No. 25-1047) coexist. When the thermal treating temperature increases to 850°C, one can find that the phases of WO_2 and β-$W_{40.9}N_{9.1}$ disappear, and a new phase of hexagonal α-W_2C (JCPDS No. 35-0776) occurs, as shown in Fig. 3(c). As shown in Figs. 3(c) and (d), with increases in thermal treating time from 5 to 10 h, the hexagonal WC becomes the dominant phase, and a very small amount of α-W_2C and cubic W (JCPDS No. 04-0806) coexist. The product obtained at 950°C for 5 h mainly consists of hexagonal WC, coexisting with a very small amount of α-W_2C, as shown in Fig. 3(e). An elevated treating temperature and a shortened treating time, e.g., at 1000°C for 2 h, can also achieve a product with major compositions of hexagonal WC and α-W_2C, as shown in Fig. 3(f). The product obtained at 1050°C for 2 h is composed of the pure hexagonal WC phase, as shown in Fig. 3(g).

Figure 4 shows the typical SEM images of the WC product obtained at 1050°C for 2 h with various magnifications. A low-magnification SEM image in Fig. 4(a) indicates that the WC product consists of spherical microparticles, which are well dispersed in a large view field. Figure 4(b) shows an enlarged SEM image, indicating that the spherical microparticles are porous aggregates with an apparent size range of 5–15 μm. A high-magnification SEM image, as shown in Fig. 4(c), indicates that the porous microparticles are loose aggregates of WC nanoparticles with a particle size of 100–250 nm. The result of laser particle size analysis indicates that the apparent particle sizes of the WC powders obtained at 1050°C for 2 h range in 4.0–18.0 μm, with a peak size of 8.6 μm. The above result is consistent with the SEM observations (Figs. 4(a) and (b)). The specific surface area of the WC powders obtained at 1050°C for 2 h is 1.7 m^2/g. Their average diameter estimated according to the specific surface area is about 200 nm, which is very close to the high-resolution SEM observation (Fig. 4(c)). The molar ratio of W to C of the WC sample obtained at 1050°C for 2 h is close to 1:1 according to the EDS spectra.

The formation process of hexagonal WC particles undergoes the following steps according to the XRD results. Firstly, the pyrolysis of the tungstate-based inorganic–organic hybrid precursor leads to the formation of tungsten oxides (e.g., WO_2), and some species containing carbon and nitrogen in the sealed quartz tube. Secondly, the species containing carbon and nitrogen react with the tungsten oxides, and form β-$W_{40.9}N_{9.1}$, α-W_2C, W, and WC. Thirdly, the phases of β-$W_{40.9}N_{9.1}$, α-W_2C, and W further react with the C-containing species, and finally form a hexagonal WC phase by elevating the reaction temperature and prolonging the reaction time. In the sealed quartz tube, the pyrolyzed organic ammonium ions emit excess C-containing species relative to the amount of W, and this is helpful for the formation of a pure WC phase. The excess C forms carbon films and carbon beads in the other end wall of the quartz tube. The above results are validated by EDS examination on the samples collected from different parts of the quartz tube. The possible chemical reactions that occur during the heat treatment depending on the heat treatment temperature can roughly be described by the following equations:

$$(C_8H_{17}NH_3)_2WO_4 \xrightarrow{C/CO/C_mH_n,\ \leq 750^\circ C} WO_2 + C + CO + NH_3 + C_mH_n \quad (1)$$

$$WO_2 \xrightarrow{C/CO/C_mH_n,\ \geq 800^\circ C} W + \alpha - W_2C + WC \quad (2)$$

$$WO_2 \xrightarrow{NH_3,\ 750^\circ - 800^\circ C} \beta\text{-}W_{40.9}N_{9.1} \xrightarrow{C/CO/C_mH_n,\ 800^\circ - 850^\circ C} W + \alpha\text{-}W_2C + WC \quad (3)$$

$$W + \alpha\text{-}W_2C \xrightarrow{C/CO/C_mH_n,\ \geq 850^\circ C} WC \quad (4)$$

IV. Conclusions

Hierarchical WC microparticles consisting of hexagonal WC nanocrystals have been synthesized by thermally treating a novel tungstate-based inorganic–organic hybrid precursor in a vacuum sealed quartz tube at 1050°C for 2 h. The as-obtained WC particles are of a unique porous and hierarchical structure, which not only makes the product easily disperse and recycle in applications, but also makes the product have a high surface area. The proposed single-source method is simple, efficient, and inexpensive for the synthesis of WC micro-/nanocrystals.

References

[1]Z. J. Lin, L. Wang, J. Z. Zhang, H. K. Mao, and Y. S. Zhao, "Nanocrystalline Tungsten Carbide: As Incompressible as Diamond," *Appl. Phys. Lett*., **95** [21] 211906, 3pp (2009).

[2]A. H. Jones and P. Roffey, "The Improvement of Hard Facing Coatings for Ground Engaging Applications by the Addition of Tungsten Carbide," *Wear*, **267** [5–8] 925–33 (2009).

[3]J. P. Bosco, K. Sasaki, M. Sadakane, W. Ueda, and J. G. G. Chen, "Synthesis and Characterization of Three-Dimensionally Ordered Macroporous (3DOM) Tungsten Carbide: Application to Direct Methanol Fuel Cells," *Chem. Mater*., **22** [3] 966–73 (2010).

[4]Y. Wang, S. Q. Song, P. K. Shen, C. X. Guo, and C. M. Li, "Nanochain-Structured Mesoporous Tungsten Carbide and Its Superior Electrocatalysis," *J. Mater. Chem*., **19** [34] 6149–53 (2009).

[5]A. Kumar, K. Singh, and O. R. Pandey, "Reduction of WO_3 to Nano-WC by Thermo-Chemical Reaction Route," *Physica E*, **41** [4] 677–84 (2009).

[6]H. Won, H. Nersisyan, and C. Won, "Combustion Synthesis of Nano-Sized Tungsten Carbide Powder and Effects of Sodium Halides," *J. Nanopart. Res*., **12** [2] 493–500 (2009).

[7]T. G. Ryu, H. Y. Sohn, K. S. Hwang, and Z. Z. G. Fang, "Plasma Synthesis of Tungsten Carbide Nanopowder from Ammonium Paratungstate," *J. Amer. Ceram. Soc*., **92** [3] 655–60 (2009).

[8]J. H. Jang, J. Kim, Y. H. Lee, C. Pak, and Y. U. Kwon, "Sonochemical Synthesis of Tungsten Carbide-Palladium Nanocomposites and Their Electrocatalytic Activity for Hydrogen Oxidation Reaction," *Electrochim. Acta*, **55** [2] 485–90 (2009).

[9]S. R. Vallance, S. Kingman, and D. H. Gregory, "Ultrarapid Materials Processing: Synthesis of Tungsten Carbide on Subminute Timescales," *Adv. Mater*., **19** [1] 138–42 (2007).

[10]E. J. Rees, C. D. A. Brady, and G. T. Burstein, "Solid-State Synthesis of Tungsten Carbide from Tungsten Oxide and Carbon, and Its Catalysis by Nickel," *Mater. Lett*., **62** [1] 1–3 (2008).

[11]C. Giordano, C. Erpen, W. Yao, B. Milke, and M. Antonietti, "Metal Nitride and Metal Carbide Nanoparticles by a Soft Urea Pathway," *Chem. Mater*., **21** [21] 5136–44 (2009).

[12]C. Ma, N. Brandon, and G. H. Li, "Preparation and Formation Mechanism of Hollow Microspherical Tungsten Carbide with Mesoporosity," *J. Phys. Chem. C*, **111** [26] 9504–8 (2007).

[13]P. Hui, F. Yuan Ping, and L. Jianyi, "Hydrogen Adsorption by Tungsten Carbide Nanotube," *Appl. Phys. Lett*., **90** [22] 223104, 3pp (2007).

[14]J. C. Lytle, N. R. Denny, R. T. Turgeon, and A. Stein, "Pseudomorphic Transformation of Inverse Opal Tungsten Oxide to Tungsten Carbide," *Adv. Mater*., **19** [21] 3682–6 (2007).

[15]D. Chen and Y. Sugahara, "Tungstate-Based Inorganic–Organic Hybrid Nanobelts/Nanotubes with Lamellar Mesostructures: Synthesis, Characterization, and Formation Mechanism," *Chem. Mater*., **19** [7] 1808–15 (2007). □